ELSEVIER

Applied Mathematical Modelling 24 (2000) 263–278

APPLIED MATHEMATICAL MODELLING

www.elsevier.nl/locate/apm

Analysis of three-dimensional flow in a cylindrical sediment oxygen demand chamber

Joseph H.W. Lee [a,*], C.P. Kuang [b], K.S. Yung [c]

[a] *Department of Civil Engineering, The University of Hong Kong, Pokfulam Road, Hong Kong, People's Republic of China*

[b] *Department of River & Harbour Engineering, Nanjing Hydraulic Research Institute, Nanjing 210024, People's Republic of China*

[c] *Hong Kong Environmental Protection Department, Hong Kong, People's Republic of China*

Received 14 May 1998; received in revised form 5 July 1999; accepted 29 July 1999

Abstract

The rate of consumption of dissolved oxygen at the bottom of a river or coastal water is often measured in situ by a sediment oxygen demand (SOD) chamber. A continuous flow is generated above the sediment, and the SOD is determined from the difference in oxygen concentrations in the inflow and outflow. The steady three-dimensional swirling laminar flow field inside a cylindrical SOD chamber previously used in field investigations is computed using the finite volume method on an unstructured tetrahedral mesh. The numerical predictions reveal a highly complicated flow characterized by (i) a mainly tangential and near-uniform flow along the circumference in the horizontal layers; (ii) significant reverse bottom currents; and (iii) strong swirl induced by the jet momentum in the vertical section. The computed scalar field suggests that good mixing is achieved within the chamber. The computed velocity and scalar field are well supported by laboratory velocity measurements using laser-Doppler anemometry (LDA), and measured concentrations in a tracer experiment. The present study elucidates the fluid mechanics of an important type of SOD chamber design often used in environmental water quality studies.

Keywords: Sediment oxygen demand; Laminar swirling flow; Computational fluid dynamics; Finite volume method; Unstructured grid; Cylindrical chamber flow; Environmental hydraulics; Dissolved oxygen; Water quality

1. Introduction

The sediment oxygen demand (SOD) is the rate of oxygen consumption exerted by the bottom sediment on the overlying water – due to both the respiration of the benthic biological communities and the biochemical degradation of organic matter. The SOD is often a major component of the dissolved oxygen (DO) budget and hence a key parameter in mathematical models of water quality [14], particularly in relatively shallow waters. The SOD is typically measured in situ by mounting a chamber device on the sediment surface; a steady water flow is created over the sediment to simulate natural hydraulic conditions. The SOD is determined from either (i) the drop in DO concentration inside the chamber with time (batch method), or (ii) the difference in DO

* Corresponding author. Tel.: +852-2859-2668; fax: +852-2559-5337.
E-mail address: hreclhw@hkucc.hku.hk (J.H.W. Lee).

0307-904X/00/$ - see front matter
PII: S0307-904X(99)00035-9

concentration in the inflow and outflow (continuous method). A large variety of chamber shapes, ranging from rectangular, cylindrical, to triangular cross-sections have been proposed. In particular, the cylindrical configuration has often been adopted (e.g. [1,9,8]).

Experiments and theory have shown that the flow velocity above the sediment can have a significant effect on the SOD measurement, even when no sediment re-suspension has been observed [7,10,17]. In addition, large differences in SOD measurements with different chambers have been noted; this has been attributed to differences in the chamber fluid mechanics (e.g. [4,13]). While the need to understand the key hydrodynamic factors affecting SOD has been recognized for some time [5,9], there have been scant studies of the hydrodynamics and mixing of SOD chambers. Typically, chamber designs have been studied using reactor ('black box') concepts supplemented by dye tracing experiments. Some limited attempts to measure point velocities by propeller, hot-film anemometry or electromagnetic current meter have been made [3,5,16]. However, the measurements were insufficient to gain a picture of the flow field inside the chamber. The numerical simulation of SOD chamber flows has hitherto not been reported.

We carry out a numerical and experimental study of the fluid mechanics of a SOD chamber of circular horizontal section; the flow is driven by a twin jet inflow discharge. The steady three-dimensional laminar flow in the SOD chamber is computed; the governing continuity and momentum equations are solved numerically using the finite volume method on an unstructured grid. The salient features of the computed flow field are presented; predicted velocities are compared with laboratory velocity measurements using laser-Doppler anemometry. The numerical solution of the full time-dependent advective diffusion equation for a passive scalar is also compared with measurements from a tracer experiment. The implications of the numerical study on SOD chamber design are discussed.

2. Theory

2.1. Cylindrical SOD chamber

Fig. 1(a) shows a schematic diagram of a SOD measurement system used to study short-term dissolved oxygen dynamics in Tolo Harbour, Hong Kong [8]. This system consists of a water-tight cylindrical SOD chamber positioned on the sea bed and connected to a data control and acquisition system on board (typically a fish-farm raft). The chamber is fabricated from a perspex cylinder of diameter 14.4 cm. The bottom of the chamber is open, which allows the SOD chamber to be inserted into the sediment, and positioned on the bed with the aid of a stabilizing plate. The chamber top is slightly tapered (to facilitate purging of gas bubbles released from the sediment), and fitted with one outlet nozzle at the centre, and two inlet nozzles. In field operation, a continuous flow Q can be generated by a peristaltic pump on board connected to the outflow nozzle by a tubing. The surrounding sea water enters the chamber through the twin inflow nozzles as two diametrically opposite jets inclined at 45° to the vertical; the outflow exits from the centre of the chamber top. This design promotes efficient mixing in the chamber, and is particularly suited for measuring transient changes of SOD during a day (caused e.g., by algal blooms and red tides). Both the dissolved oxygen concentration of the inflow, C_i (g/m^3), and that of the outflow after sediment consumption, C_o, can be measured. If the surface area of the sediment enclosed by the chamber is A, then a steady mass balance results in, after proper unit conversion, SOD (g/m^2/d) $= Q(C_i - C_o)/A$. Both the inlet and outlet nozzle have an internal diameter of 4 mm; the chamber top and the inlet jet discharge point are located at 10 and 7 cm above the sediment, respectively. The distance between the two inflow nozzles is 8.4 cm.

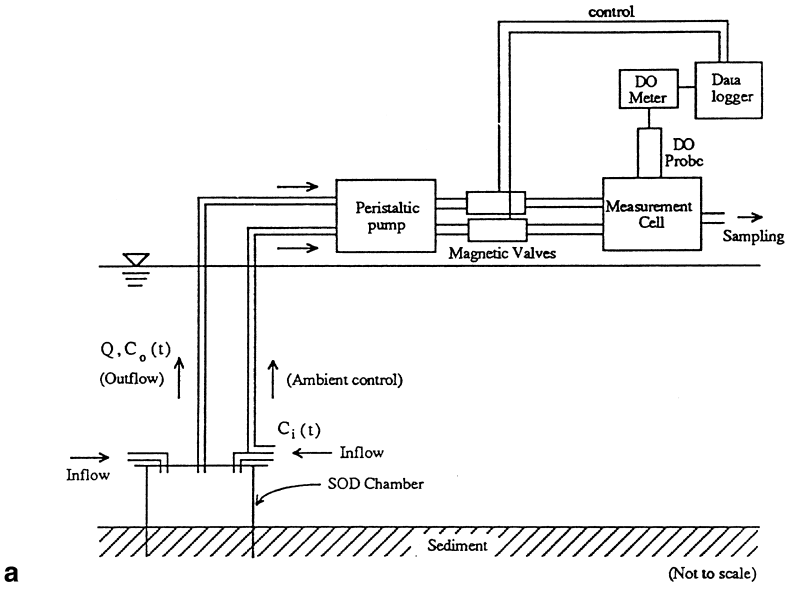

a

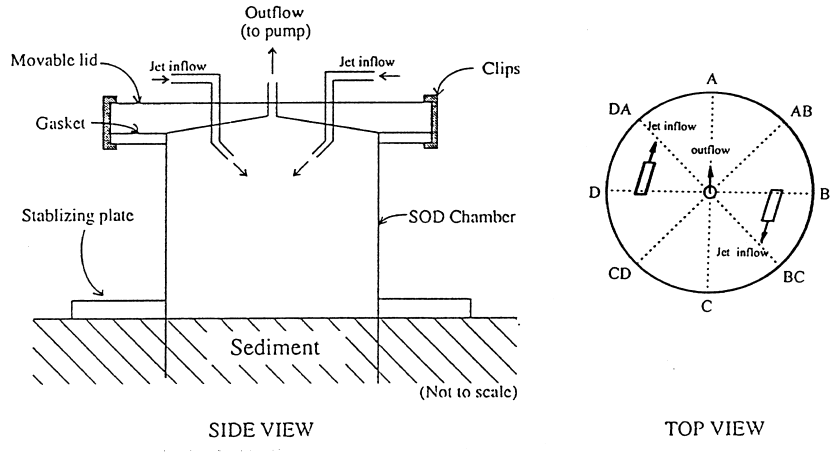

b

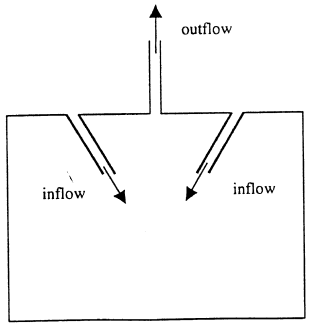

c

Fig. 1. Continuous-flow in situ sediment oxygen demand (SOD) measurement system: (a) schematic flow diagram; (b) cylindrical SOD chamber; (c) section view of computational domain.

The present numerical and experimental studies are performed for a replicate of the perspex chamber having the same inflow/outflow arrangements but with, however, a solid bottom and a horizontal top. Further, the inflow nozzle is numerically represented by a straight inlet pipe (inclined at 45°) ending at the same jet discharge location (Fig. 1(c)). The velocity field inside the chamber is studied for a steady water flow of $Q = 240$ ml/min; this throughflow is to produce over–bottom velocities of the order of 1 cm/s (commonly encountered in semi-enclosed tidal bays). At this flow rate, the inflow enters the chamber as a laminar jet; the Reynolds number based on the jet velocity ($V_j = 0.16$ m/s) and diameter is around 640. Our objective is to obtain, through numerical computations and experiments, a basic understanding of the SOD chamber flow.

2.2. Governing equations

The three-dimensional flow in the cylindrical chamber is computed numerically by solving the full Navier–Stokes (NS) equations. For $t \geqslant 0$, a constant flow 240 ml/min is applied to the inlet; the chamber flow is numerically computed until steady conditions are obtained.

We adopt the following equations for constant density incompressible steady flow:

$$\frac{\partial U_i}{\partial x_i} = 0, \tag{1}$$

$$U_j \frac{\partial U_i}{\partial x_j} = -\frac{1}{\rho}\frac{\partial p}{\partial x_i} + \frac{\partial}{\partial x_j}\left(v\left(\frac{\partial U_j}{\partial x_i} + \frac{\partial U_i}{\partial x_j}\right)\right), \tag{2}$$

where U_i is the fluid velocity in x, y and z directions, ρ the density, p the dynamic pressure, and v is the molecular viscosity. In addition to the flow equations, the study of mixing inside the chamber necessitates the calculation of a passive scalar field from the advective diffusion equation:

$$\frac{\partial C}{\partial t} + U_j \frac{\partial C}{\partial x_j} = \frac{\partial}{\partial x_i}\left(D\frac{\partial C}{\partial x_i}\right), \tag{3}$$

where D is the molecular diffusivity for the passive scalar.

2.3. Initial and boundary conditions

By virtue of periodic symmetry, the numerical solution is sought for one half of the flow domain, $x \geqslant 0$ (i.e. the half-space to the right of line AC in Fig. 1(b)). This flow has rotational periodic symmetry in that the flow across a line OA (where O is the centre of the cylinder), for example, is the same in magnitude but diametrically opposite to the flow across the line OC. The flow at a periodic boundary is treated as though the opposing periodic plane is a direct neighbour to the cells adjacent to the first periodic boundary. Thus, when calculating the flow through the periodic boundary adjacent to a fluid cell, the flow conditions at the fluid cell adjacent to the opposite periodic plane are used.

At the inlet boundary, $Q = 240$ ml/min and (for the tracer experiment) a scalar concentration of $C_i(t) = 1.0$ is imposed for $t \geqslant 0$. At the outlet boundary, the flow is full-developed, normal gradients of all variables are set to zero. At the wall boundary, the no-slip condition is imposed. The inflow pipe is treated as a 'two-sided zero thickness wall', which forms the interface between two different fluid regions. The no-slip condition is also used for this kind of 'two-sided zero thickness wall'. Zero velocity and pressure are prescribed as initial values. For computation of tracer concentration, $C(t = 0) = 0$ is prescribed.

2.4. Computational procedure and details

The governing equations are solved numerically using the finite volume method [11] as embodied in the FLUENT/UNS code (Fluent Inc. 1996). The equations are discretized on a three-dimensional, unstructured mesh composed of tetrahedral cells on which Cartesian velocities and other variables are defined at the cell centre [12]. Cell-face dependent variables are interpolated from the cell centre values using a second order upwind scheme. The set of discretized simultaneous algebraic equations is solved by an algebraic multigrid linear equation solver [6]. A first order accurate unconditionally stable implicit scheme is used for time discretization, with all spatial derivatives and other terms treated in a fully implicit manner. At each time step/iteration, the discretized equations are solved using the SIMPLEC algorithm for velocity–pressure correction [15]. In the calculations for velocity field, no under-relaxation of pressure is required, while a factor of 0.65 is adopted for velocities. Convergence is declared when the scaled residual R is less than 5×10^{-4} for every equation. About 1400 iterations are required for convergence. After the steady flow field has been obtained, the unsteady 3D scalar field inside the chamber due to a step increase of concentration in the inflow is computed. For this calculation, $C(t = 0) = 0$, and $C_i(t) = 1.0$ is prescribed for the inflow for $t \geqslant 0$. No under-relaxation of concentration, density and viscosity is adopted. The time step varies from 1 to 6 s. At each time step, a maximum of 20 iterations are required for convergence, when the scaled residual in the scalar mass conservation equation is less than 5×10^{-4}.

Fig. 2(a) shows the unstructured tetrahedral mesh formed using the FLUENT/TGrid code (Fluent Inc. 1996). First, boundary surface meshes are generated by decomposing the domain into a set of packed convex polygons (Delaunay triangulation). This can be achieved by specifying the nodes along the bounding curves which form boundary surfaces, and the node density on different parts of the surface. The mesh can then be generated only using the boundary nodes with an iterative node generation scheme, followed by edge swapping and Laplace smoothing operations to improve mesh quality. For the cylindrical chamber, the surface mesh has 10,598 triangular cells and 5301 nodes. The surface meshes of the wall surface at inflow end, bottom surface, periodic symmetry surface, and inlet surface are also shown. After generating the surface mesh, the interior mesh composed of tetrahedral cells can be generated using the approach proposed by Bowyer [2]. Convergence tests showed that about 40,000 cells would be needed, when computed average velocities in selected planes differ by less than 2%. All calculations shown herein are obtained on a computational mesh that divides the cylindrical chamber into 54,276 tetrahedral cells (consisting of 11,886 nodes, 103,183 triangular faces). The average cell volume, face area and cell skewness are 1.50×10^{-8} m^3, 1.20×10^{-5} m^2 and 0.32, respectively; the length of the triangular mesh varies from 0.1 to 0.9 cm.

3. Numerical results and analysis

The numerical results show that a highly complicated flow with significant swirl is generated inside the cylindrical SOD chamber. Fig. 3 shows the computed horizontal velocity field at different depths above the bottom; for each depth the velocity vectors along different radial transects are shown. It can be seen that the flow is mainly tangential and fairly uniform in the layers above the inflow jet ($y > 7$ cm) except close to the centre and boundaries. Similarly, the flow is mainly tangential and nearly uniform circumferentially in the layers between the inlet and 1 cm layer above the bottom. The position of the maximum horizontal velocity near the outer circumference shifts following the inflow discharge jet direction. For example, at $y = 5$ cm, the maximum

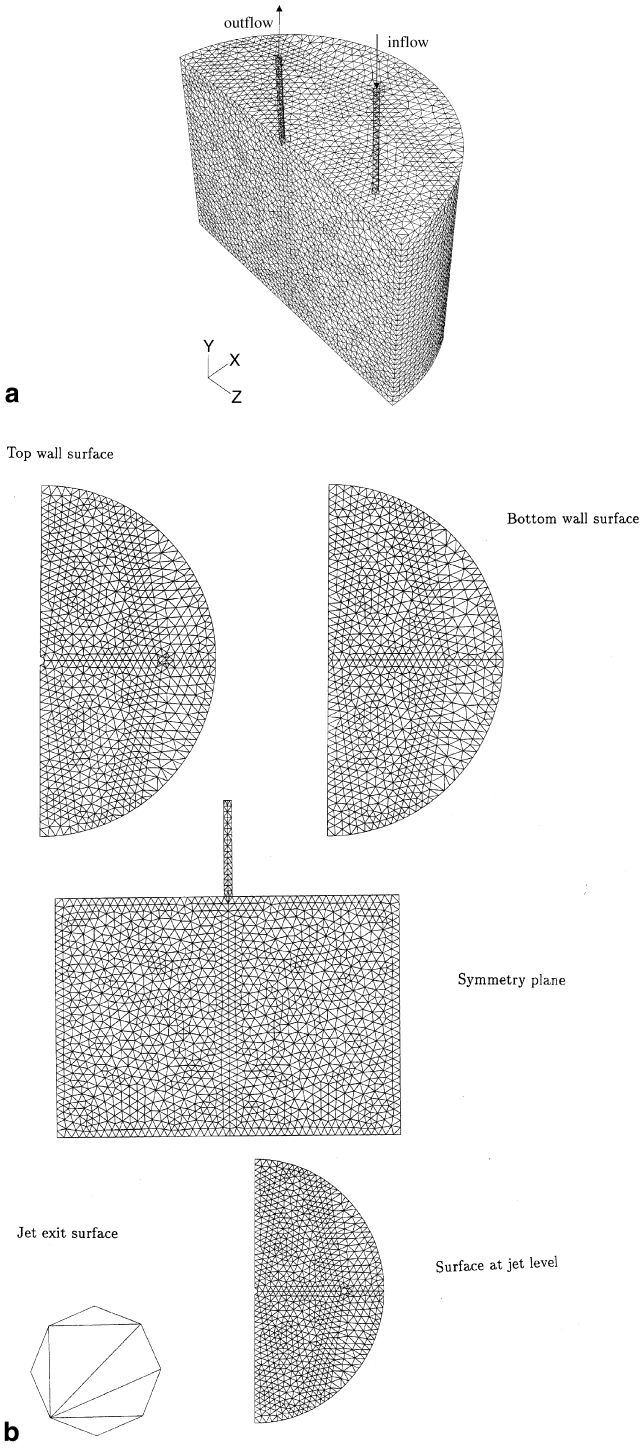

Fig. 2. (a) Outline of unstructured tetrahedral mesh for SOD chamber computation. (b) Surface mesh for wall surface at inflow end, bottom wall, symmetry plane, and surface at jet inflow level.

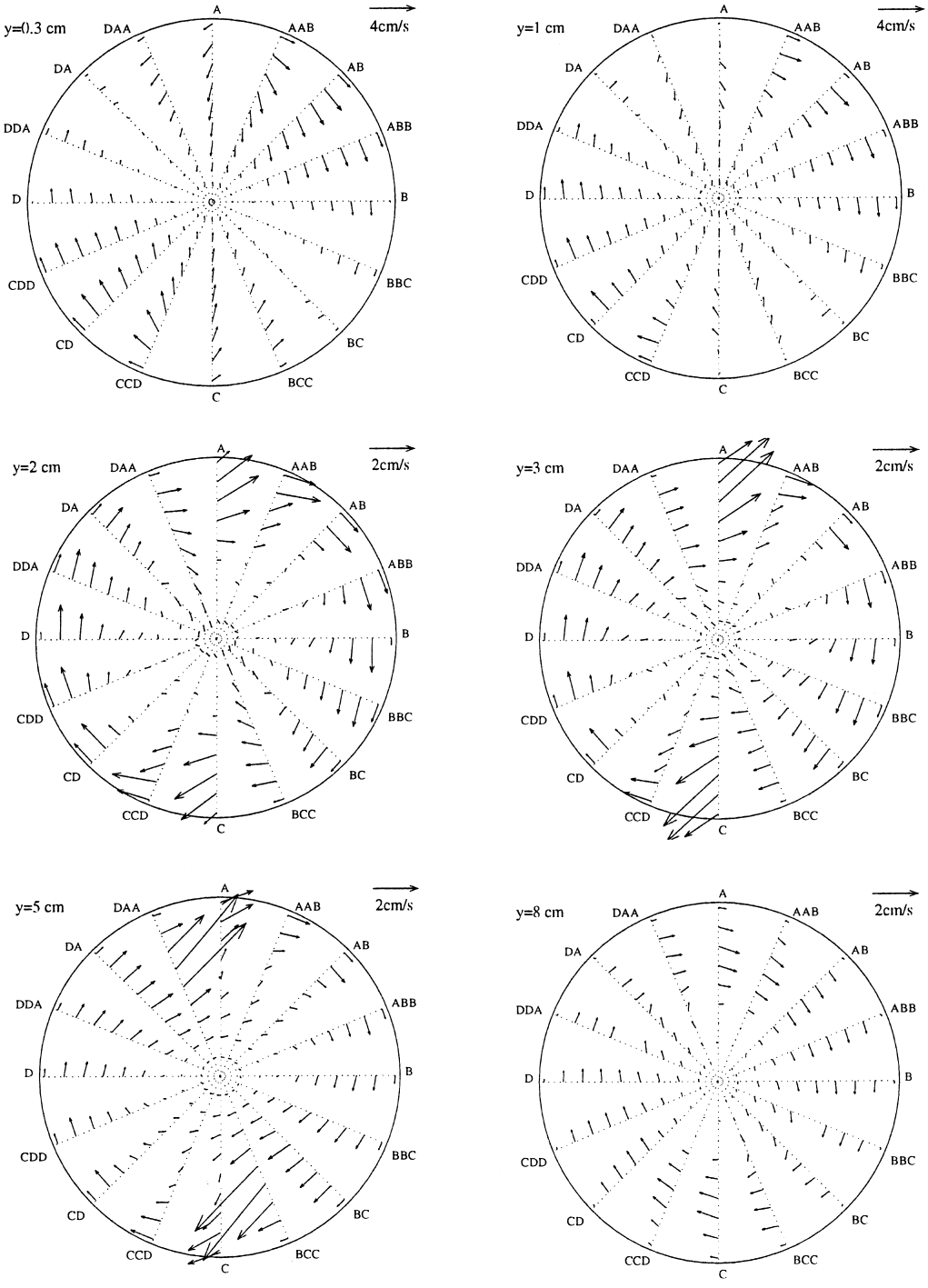

Fig. 3. Computed velocity field in selected horizontal planes.

horizontal velocity is found near the radial transect BCC; the location shifts to transect C at $y = 2$ cm. A weak swirl exists in front of the location of maximum horizontal velocity. Further, in the layers close to the bottom ($y < 1$ cm), significant reverse return flows (opposite to the jet direction) are predicted. The closer the bottom of the chamber, the stronger is the reverse return

flow. At $y = 0.3$ cm, the computed maximum horizontal velocity is about 2.5 cm/s along AAB–AB (between transects AAB and AB), at radial position $r = 6.2$ cm. From transect A–AAB to BC, the flow is mainly tangential and follows the direction of the jet. The velocity decreases progressively from section A–AB to BC to around 0.4 cm/s at the outer circumference; the flow is mainly radially inwards close to the centre. For transect BC–BCC to C, the flow is opposite to the main flow and travels towards the centre. The horizontal (x-) and transverse (z-) velocity, (u, w), varies from -0.8 to 1.5, and from -1.7 to 1.9 cm/s, respectively, with a mean horizontal velocity of 1.24 cm/s. At 1 cm layer above the bottom, the reverse flow is clearly not as strong and $u = -0.7$ to 1.9 cm/s, $w = -1.0$ to 1.8 cm/s, with a mean horizontal velocity of 1.03 cm/s. Representative velocities for other layers (excluding the velocity inside the inflow pipe) are shown in Table 1); the average horizontal over–bottom velocity for $y = 1$ to 3 cm is 0.94 cm/s.

The computed velocity in selected vertical sections (Fig. 4) reveals clearly a jet-induced swirl – e.g. at the corner in vertical section (A) in front of the inflow jet (maximum velocity about 4.2 cm/s), with a weak backflow in the upper region of the chamber. Following the main flow (e.g., from section A to BBC), the centre of the swirl moves upwards and towards the centre of the chamber. The vertical (y) velocity is comparable to the horizontal velocity, and varies from -3.7 to 3.1 cm/s – suggesting good mixing in the chamber. Representative vertical and radial velocities are shown in Table 2) (excluding the velocity inside the inflow and outflow pipes).

The computed shear stress at the bottom wall of the SOD chamber, which influences the diffusive mass transfer at the sediment–water interface, is shown Fig. 5. It can be seen that the twin shear stress maxima (around 0.02 N/m^2) are located close to the outer wall, near AAB and CCD. The distribution of shear stress is generally in accordance with near bottom velocities.

Additional insights into the flow pattern can be obtained from Lagrangian pathlines. Based on the 3D computed velocity field for $Q = 240$ ml/ min, the trajectory of a particle released inside the chamber can be constructed. A fixed space step of 0.001 m is used; the position of the particle at the end of a step can be calculated by interpolating the velocity at the original position. Fig. 6 shows the pathlines for a particle released from four vertical sections at different depths: at level of inflow in section B, $y = 5$ cm in section BC, $y = 3$ cm in section C, and close to the bottom in section CD. From Fig. 6, the mixing pattern as induced by the jet through the swirling motion is clearly seen. The flow is seen to leave the chamber from the center of all vertical sections. The pathlines indicate that good mixing is achieved inside the chamber.

After the steady flow field is obtained, the unsteady 3D scalar field in the chamber is computed for the step increase in inflow concentration. Except for small times and very close to the inflow jet nozzles, the computed scalar field (not shown) indicates negligible concentration gradients (of the

Table 1
Computed velocity at different depth layers (cm/s)

y (cm)	x-velocity (u) range	z-velocity (w) range	$\sqrt{u^2 + w^2}$	
			Range	Mean
0.3	−0.8 to 1.5	−1.7 to 1.9	0.04 to 2.5	1.24
1	−0.7 to 1.9	−1.0 to 1.8	0.07 to 2.3	1.03
2	−1.8 to 2.0	−1.2 to 1.5	0.03 to 2.1	0.90
3	−2.5 to 2.5	−2.3 to 2.3	0.03 to 3.3	0.89
4	−2.0 to 2.0	−2.0 to 2.0	0.03 to 2.6	0.89
5	−2.8 to 1.4	−0.8 to 3.3	0.05 to 4.3	0.85
6	−2.3 to 1.3	−0.2 to 2.6	0.07 to 3.5	0.75
7	−3.0 to 1.1	−0.4 to 3.1	0.04 to 4.3	0.61
8	−0.9 to 0.9	−0.3 to 0.6	0 to 1.0	0.52
9	−0.6 to 0.6	−0.4 to 0.6	0.02 to 0.7	0.46

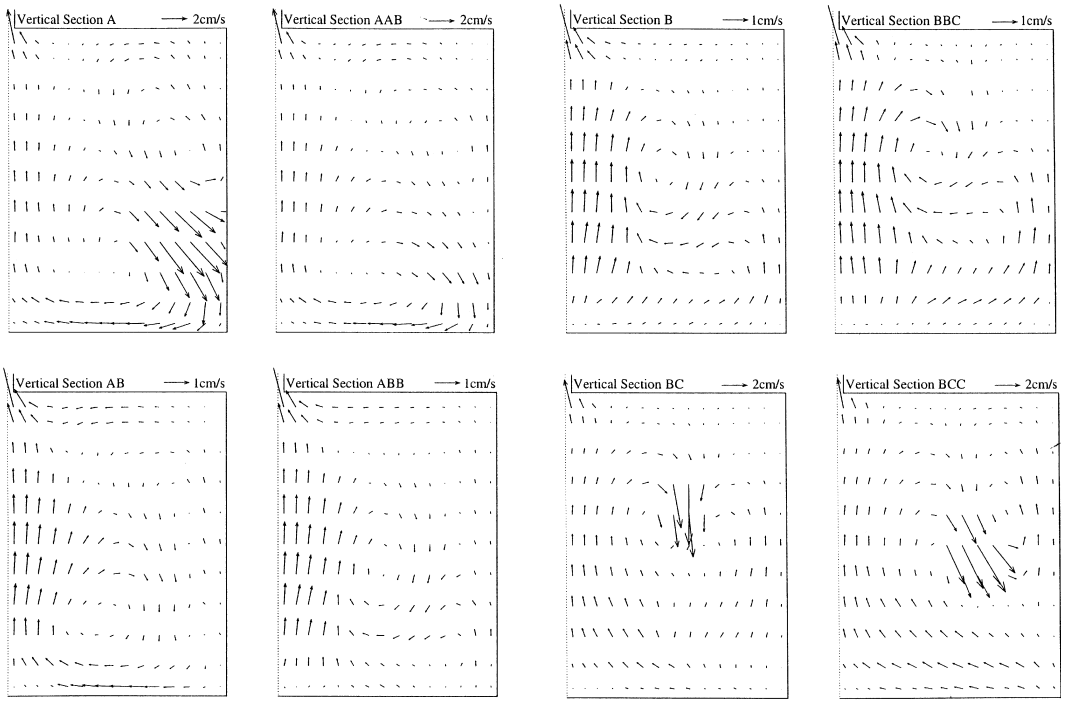

Fig. 4. Computed velocity field in selected vertical sections.

Table 2
Computed velocity at different vertical sections (cm/s)

Vertical sections	Radial-velocity (u_r) range	y-velocity (v) range	$\sqrt{u_r^2+v^2}$	
			Range	Mean
A	−1.5 to 2.4	−2.7 to 2.7	0.02 to 4.2	0.72
AAB	−1.5 to 0.7	−1.2 to 2.8	0 to 2.9	0.47
AB	−0.8 to 0.3	−0.3 to 3.0	0 to 3.1	0.32
ABB	−0.8 to 0.2	−0.3 to 3.1	0.02 to 3.2	0.30
B	−0.8 to 0.2	−0.3 to 3.0	0.01 to 3.1	0.32
BBC	−0.7 to 0.4	−0.4 to 2.5	0 to 2.6	0.35
BC	−0.6 to 0.7	−0.5 to 2.3	0.01 to 4.8	0.51
BCC	−0.8 to 2.2	−3.7 to 2.4	0.02 to 4.3	0.63

order of a few percent) in the main body of the chamber. Fig. 7 shows the predicted time variation of the concentration in the outflow, $C_o(t)$ (approximately the same as the average concentration inside the chamber). Note that for a fully mixed system or 'reactor', a mass balance gives $V(dC/dt) = -QC + QC_i$, where $C(t), C_i$ are the concentrations in reactor and inflow, respectively, V is the volume of reactor, and Q is the steady throughflow. The theoretical retention or residence time of the tracer in the system (the 'time constant') is then $T = V/Q$; i.e. for initial concentration of $C(t=0) = C_*$ and no source input, $C_i = 0$, $C(t) = C_* e^{-t/T}$. Similarly, for step increase of inflow concentration, $C_i = 1.0$ for $t \geqslant 0$, the solution is $C(t)/C_i = 1 - e^{-(Q/V)t}$. i.e. the concentration in the system increases from 0 to 1.0 over a period of time. Fig. 7 shows that the computed concentration response to a step increase of tracer concentration can be well described by the theoretical normalized tracer concentration curve, $C(t)/C_i = 1 - e^{-t/T}$.

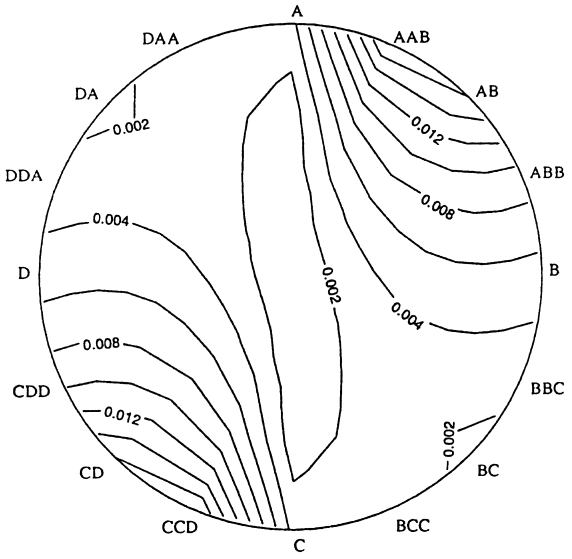

Fig. 5. Computed shear stress distribution at the bottom of SOD chamber (N/m^2).

4. Comparison with experiments

4.1. Velocity measurement

A hydraulic experimental study was carried out with a laboratory model of the cylindrical chamber. Fig. 8(a) shows the experimental set-up for the SOD chamber. The chamber is made of perspex with exactly the same dimensions, and with a fixed bottom. A steady water flow ($Q = 240$ ml/min) was supplied by a constant head tank and entered the chamber through the inlet; the flow-through rate in the closed system was monitored by a calibrated rotameter. The outlet of the chamber was connected to a drain tank which returned the flow to the source tank. The steady three-dimensional velocity field inside the chamber was measured by laser-Doppler anemometry (LDA), using a 3W Spectra Physics argon ion laser and a two-component DISA optical system. The fluid was seeded with a small amount of 'Optimage' PIV powder with nominal diameter of 30 μm and specific gravity 1.00 ± 0.02. The LDA system was operated in forward scatter mode. In our study about 1000–3000 validated samples were used at each measurement point, with a maximum period of 3 min. To determine the three velocity components (tangential, radial and vertical) at a point using the 2-component LDA system, two configurations were used. As shown in Fig. 8(b), the vertical and tangential velocity components were measured simultaneously, with the laser beams entering from the side of the chamber. To compensate for the diffraction effects of the curvature of the chamber which affect the crossing of the laser beams, the whole chamber was submerged in water inside a square perspex box. Using the 2-D traversing system, the probe-volume can be moved in the vertical and radial directions and the velocity field in a vertical plane can be measured. The chamber can be rotated (along the centreline of the chamber itself) for measurement of different vertical planes. To measure the tangential and radial components, the laser beams were made to enter from the chamber bottom.

As the cylindrical chamber is rotationally periodic, measurements were made for only one-half of the chamber (selected velocity profiles were measured to check the periodicity of flow). Velocity measurements were made in four radial sections, A, AB, B, BC, at 45° intervals. In each section,

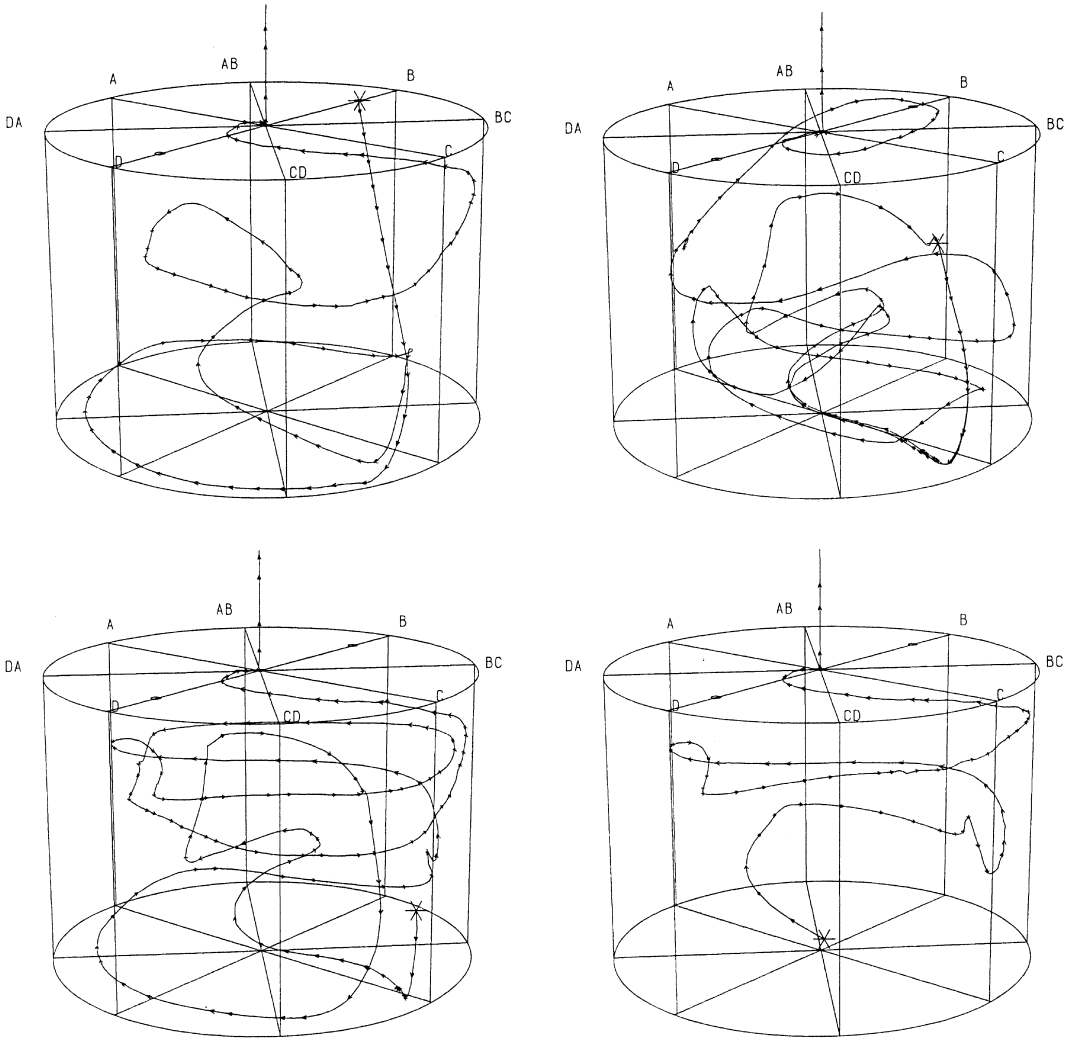

Fig. 6. Lagrangian pathlines of particles released at different starting points (starred locations).

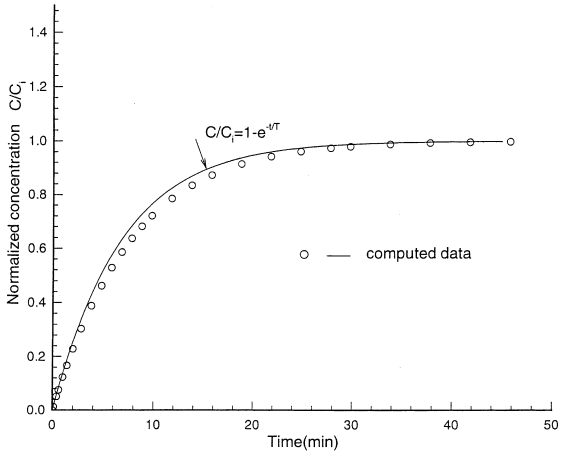

Fig. 7. Computed time variation of tracer concentration due to step increase of inflow concentration.

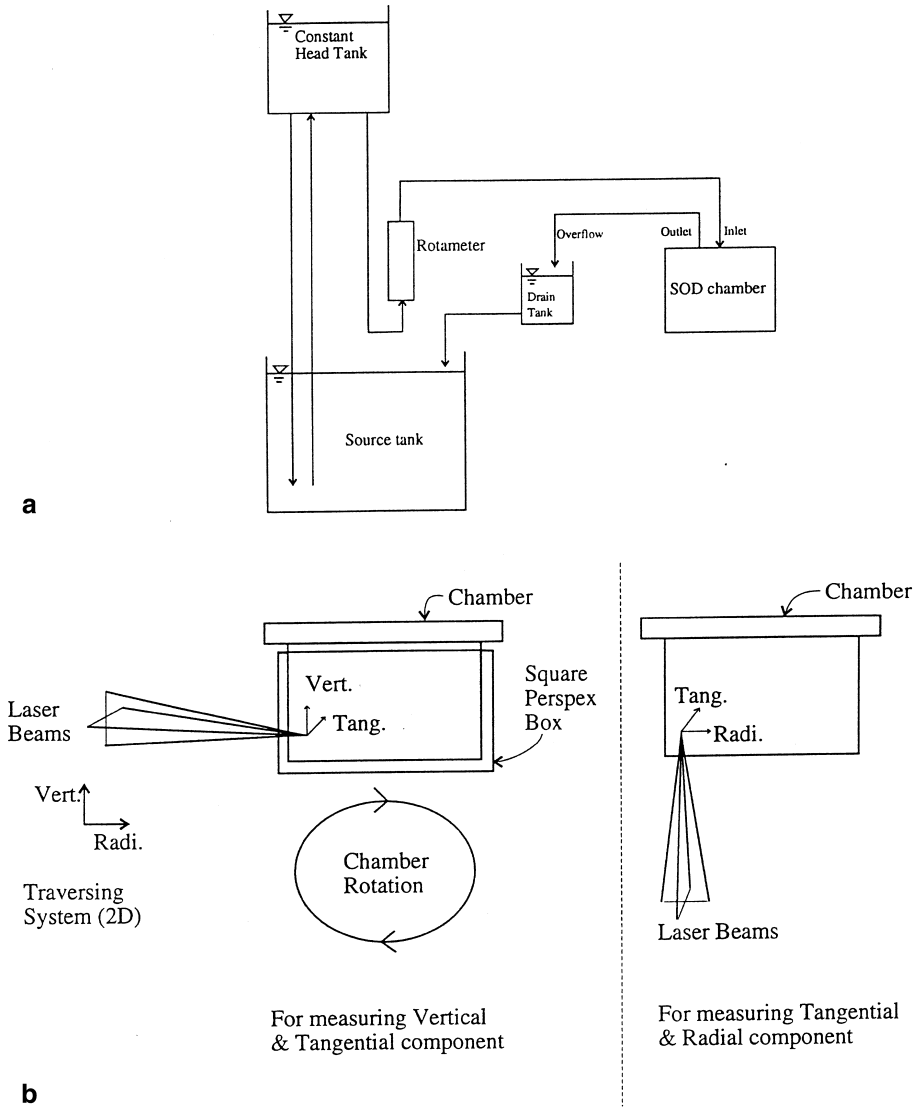

Fig. 8. (a) Experimental set up for velocity measurement. (b) LDA measurement configuration.

velocity was measured at a number of depths and radial positions. Figs. 9 and 10 show the observed velocity field at different horizontal and vertical sections, respectively. The mixing and retention time of the chamber was also studied using DO as a tracer. The chamber was first fed with a steady flow of 240 ml/min at a uniform low concentration. The inlet of the chamber was then switched to receive a continuous source of high uniform DO concentration at the same flow at $t \geqslant 0$. Fig. 11 shows the measured time variation of DO concentration of the chamber outflow. The reverse experiment (i.e. with high initial DO and switched to step input of low DO) was also done. Further experimental details can be found in [19].

4.2. Comparison of numerical predictions and experiments

Similar to the numerical calculations, the horizontal velocity measurements (Fig. 9) show that the flow is mainly tangential and nearly uniform along the circumference. Predicted horizontal

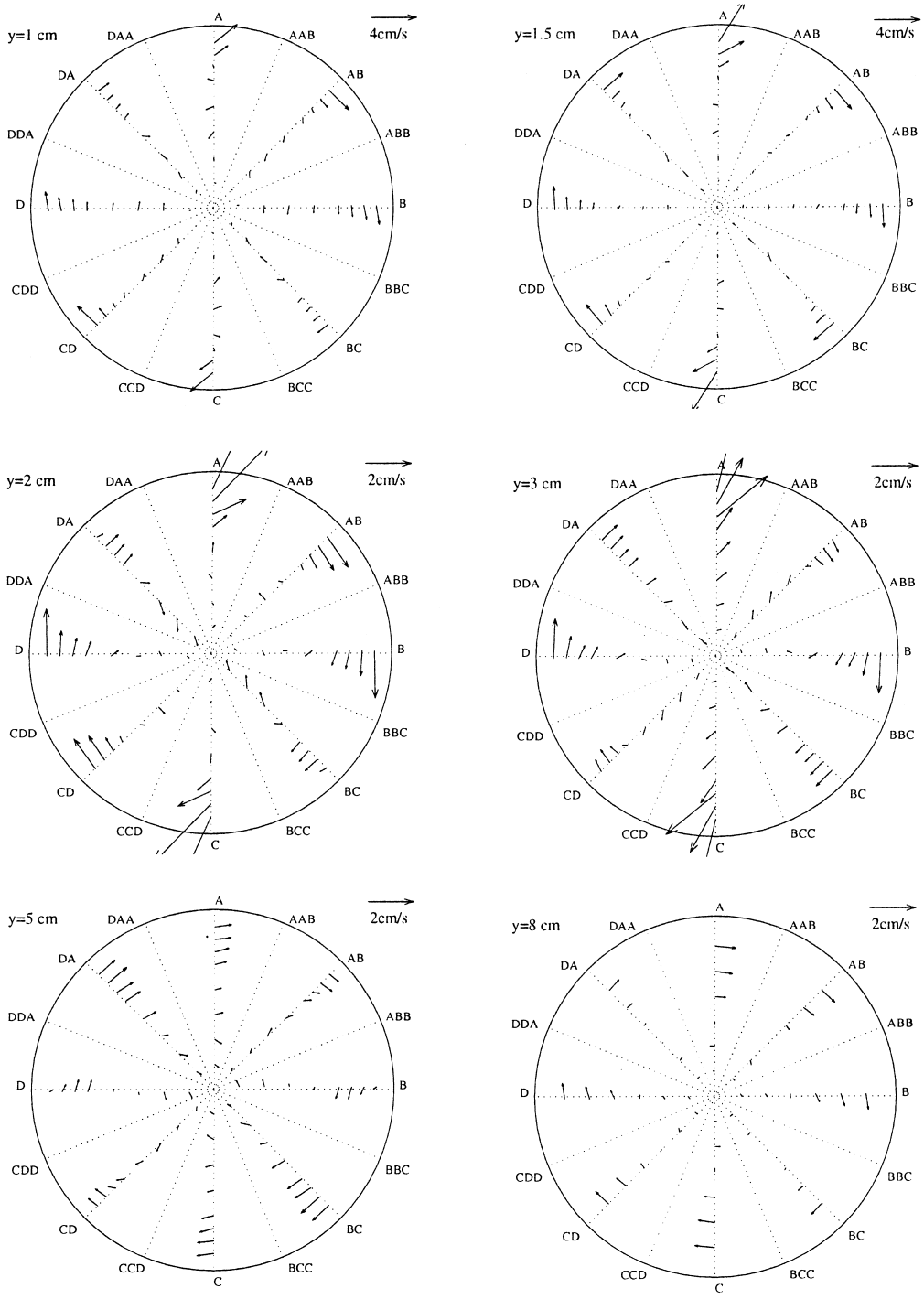

Fig. 9. Observed velocity field in different horizontal planes.

velocities also compare favourably with the measurements. For $y = 1$ cm layer, the measured horizontal velocity varies from 0.03 to 2.59 cm/s, with a mean of 0.82 cm/s. On the other hand, the computed horizontal velocity varies from 0.04 to 2.5 cm/s, with a mean of around 1.0 cm/s. The velocity observations in the vertical section (Fig. 10) reveal a strong swirl induced by the

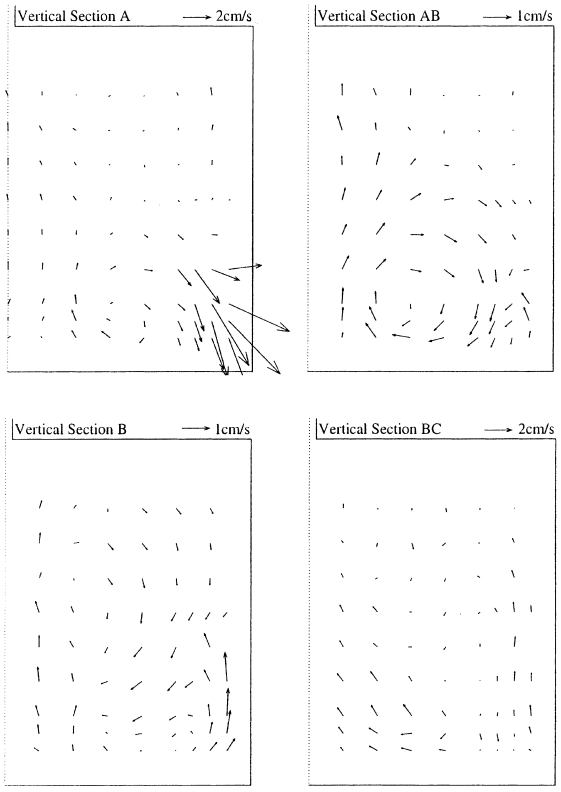

Fig. 10. Observed velocity field in different vertical sections.

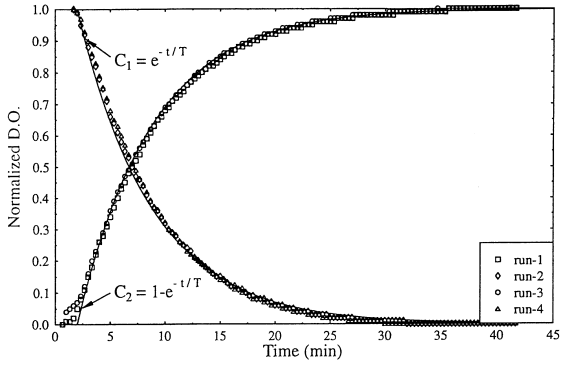

Fig. 11. Measured concentration-time response in tracer experiment.

inflow jet. The predicted flow in sections A, AB, B, and BC are well borne out by the observations. In summary, the major predicted flow features are, at least qualitatively, supported by the experiments. It should be noted that the measurement accuracy in the low velocity water flow, given the flow and measurement configuration, is probably of the order of 0.2–0.4 cm/s. Further, discrepancies of predicted versus measured flow details may also be related to the imperfect alignment of the small inflow nozzle, and the fact the LDA measurement was hampered by the presence of the inlet nozzles, and the high noise level near the bottom boundary. In any case, the calculations have captured the characteristic flow features of the cylindrical chamber. In the experimental tracer study, the measured time variation of outflow DO concentration (Fig. 11)

also indicates good mixing; the theoretical response as predicted numerically is followed after an initial time delay of the tracer arrival of about 2 min.

5. Concluding remarks

A numerical and experimental study of the fluid mechanics of a cylindrical SOD chamber has been carried out. The numerical computations reveal several distinct flow features: (i) a mainly tangential and near uniform flow along the circumference in the horizontal layers; (ii) significant reverse bottom currents; and (iii) strong swirl induced by the jet momentum in the vertical section. Good mixing is achieved in the chamber. The salient features of the predicted flow and mixing are well supported by point velocity measurements and tracer experiments.

This study demonstrates that the water currents above the sediment surface inside a SOD chamber are highly dependent on the chamber design. On the basis of this study, it is not surprising then that the SOD measured by chambers of different shapes can be quite different. While the degree of mixing can be obtained from dye tracing experiments, important flow details (e.g. the strong reverse flows near the bottom) and useful design information (e.g. the average over–bottom velocity as a function of through flow Q) can best be determined by a detailed CFD study. The present results suggest that SOD chambers should not solely be designed on the basis of residence times; an idea of the flow field can often be beneficial. The hydraulics of both rectangular and triangular chambers have also been studied; further details and related field measurements of SOD and algal dynamics can be found in [8,19].

Acknowledgements

This work was supported by the Hong Kong Research Grants Council and in part by a Postdoctoral Fellowship from the University of Hong Kong. All computations were performed on an IBM RISC System/6000 3CT workstation.

References

[1] G.T. Bowman, J.J. Delfino, SOD techniques: A review and comparison of laboratory and in situ systems, Water Res. 14 (1980) 491–499.
[2] A. Bowyer, Computing dirichlet tessellations, Comput. J. 24 (2) (1981) 162–166.
[3] W.R. Boynton, Influence of water circulation rate on in situ measurements of benthic community respiration, Marine Biol. 65 (1981) 185–190.
[4] W.S. Davis, L.A. Fay, C.E. Herdendorf, Overview of USEPA/CLEAR Lake Erie sediment oxygen demand investigations during 1979, J. Great Lakes Res. 13 (4) (1987) 731–737.
[5] C.W. Hickey, Benthic chamber for use in rivers: testing against oxygen mass balances, J. Environ. Engrg. ASCE 114 (4) (1988) 828–845.
[6] B.R. Hutchinson, G.B. Raithby, A multigrid method based on the additive correction strategy, Numer. Heat Transfer 9 (1986) 511–537.
[7] A. James, The measurement of benthal respiration, Water Res. 8 (1974) 955–959.
[8] J.H.W. Lee, K.S. Yung, P.P.S. Wong, Sediment oxygen demand and algal dynamics, Adv. Hydrosci. Engrg. (The University of Mississippi) 1A (1993) 309–316.
[9] P.J. Murphy, D.B. Hicks, In situ method for measuring sediment oxygen demand, Sediment Oxygen Demand, Processes, Modeling and Measurement, Institute of Natural Resources, University of Georgia, Athens, Georgia, USA, 1986, pp. 307–322.
[10] Y. Nakamura, H.G. Stefan, Effect of flow velocity on sediment oxygen demand, J. Environ. Engrg. ASCE 120 (5) (1994) 996–1016.

[11] S.V. Patankar, Numerical Heat Transfer and Fluid Flow, Hemisphere, New York, 1980.
[12] W. Rodi, S. Majumdar, B. Schoenung, Finite volume methods for two-dimensional incompressible flows with complex boundaries, Comput. Methods Appl. Mech. Engrg. 75 (1989) 369–392.
[13] W.J. Snodgrass, L.A. Fay, Values of sediment oxygen demand measured in the central basin of Lake Erie, 1979, J. Great Lakes Res. 13 (4) (1987) 724–730.
[14] R.V. Thomann, J.A. Mueller, Principles of Surface Water Quality Modeling and Control, Harper & Row, New York, 1987.
[15] J.P. Van Doormaal, G.D. Raithby, Enhancements of the SIMPLE method for predicting incompressible fluid flows, Numer. Heat Transfer 7 (1984) 147–163.
[16] R.C. Whittemore, Interfacial velocity effects on the measurement of sediment oxygen demand, Stream Improvement Technical Bulletin, No. 317, NCASI, 1978.
[17] R.C. Whittemore, The significance of interfacial water velocity on the measurement of sediment oxygen demand, Sediment Oxygen Demand, Processes, Modeling and Measurement, Institute of Natural Resources, University of Georgia, Athens, Georgia, USA, 1986, pp. 63–74.
[18] R.S.S. Wu, A respirometer for continuous, in situ, measurements of sediment oxygen demand, Water Res. 24 (3) (1990) 391–394.
[19] K.S. Yung, Sediment oxygen demand in coastal waters, Ph.D. thesis, The University of Hong Kong, Hong Kong, China, 1994.